

# Supplemental Material for “First simultaneous measurement of differential muon-neutrino charged-current cross sections on argon for final states with and without protons using MicroBooNE data”

This Letter shares the same event reconstruction, event selection, model validation, fake data studies, systematics and unfolding procedure as [1]. Additional details and studies can be found there and in its accompanying Supplemental Material. The data release is identical in this Letter and [1] and includes measurements from both manuscripts. A single covariance matrix is included in this data release. It contains inter-variable correlations as is obtained with the blockwise formulation of the unfolding described in [2] and in the main text of [1]. More details on the data release are in Sec. IV.

## I. 2D SMEARING AND EFFICIENCIES

The section presents the smearing matrices for the 2D  $\{\cos\theta_\mu^{rec}, E_\mu\}$  distribution. The efficiency of the  $\nu_\mu$ CC selection as a function of the same variables is also shown. The binning used for these plots is the same as used for  $S$  in the cross section extraction and is identical between reconstructed and true bins. All bins are equal width and do not represent the physical width of the energy and angle bins. The bins are in angular slices that go from backwards on the left to forwards on the right with increasing energy bins within each slice. More information on the binning can be found in Sec. IV.

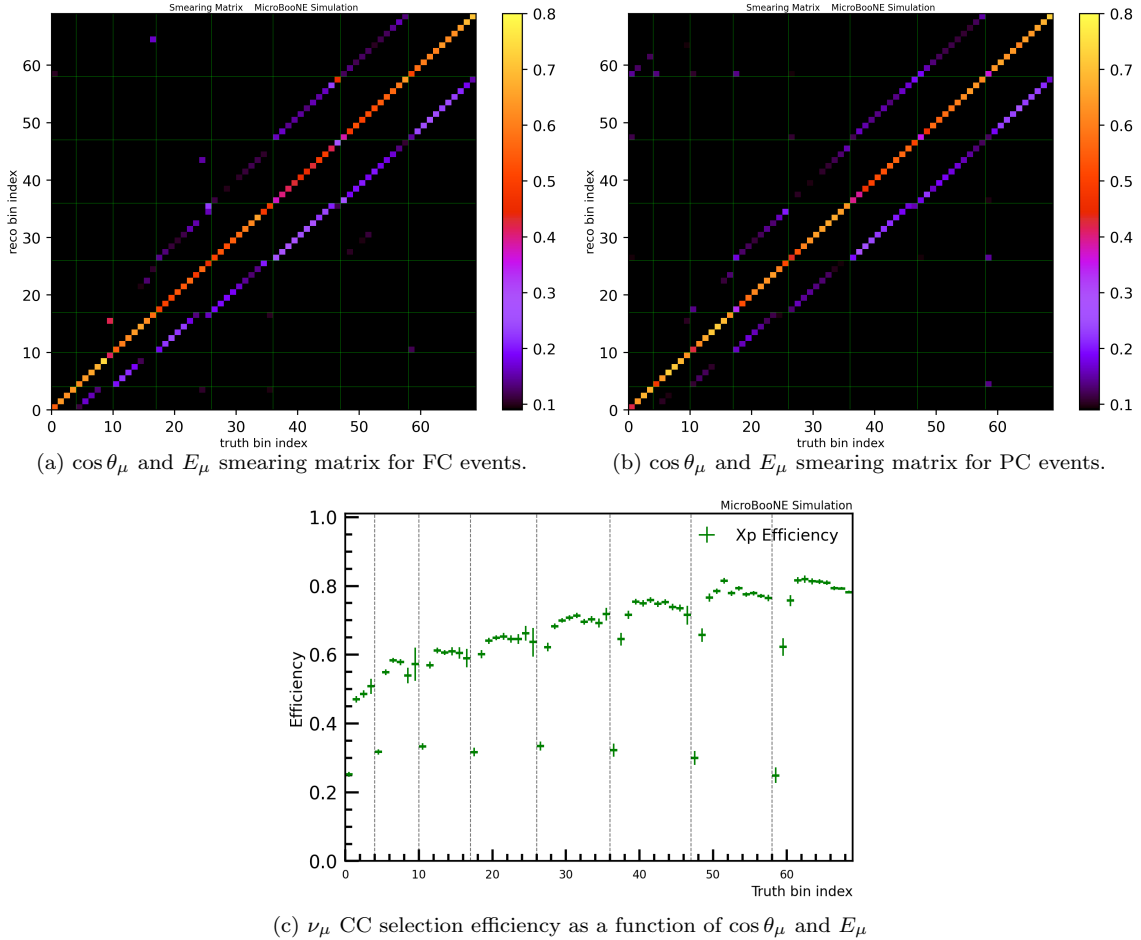


FIG. 1: Smearing matrix for the double differential measurement of  $\cos\theta_\mu$  and  $E_\mu$  for FC events (a) and PC events (b). All columns have been normalized to one. The green lines indicate the different angular slices. (c) Vectors efficiency of the  $\nu_\mu$ CC selection for each true  $\cos\theta_\mu$  and  $E_\mu$  bin in the double differential measurement. The dotted lines indicate the different angular slices. In all plots, the true and reconstructed bins are the same as those on  $S$  in the cross section extraction but are all equal width and do not represent the physical width of the energy and angle bins.

## II. FAKE DATA STUDIES

Fake data studies (FDS) were conducted to test the robustness of the model validation, derivation of the additional reweighting uncertainty and cross section extraction. For the FDS presented here, a NuWro MC sample was propagated through the MicroBooNE simulation and reconstruction chain in the same way as the nominal  $\mu$ BooNE tune MC, after which it is treated identically to real data. The purpose of this FDS is to serve as a case study of how the model validation is able to detect relevant mismodeling thereby allowing it to be mitigated via the addition of a (fake-)data-driven reweighting uncertainty obtained as described in Sec. VII of [1]. With this overall procedure, the cross section results presented in this study were not biased beyond their uncertainties. Note that the additional uncertainty derived for this FDS is not applied to real data, it is specific to the context of this FDS.

Because the fake data and MC prediction use the same detector and flux simulations, uncertainties due to beam exposure, number of targets, detector, fluxes, and reinteractions are fully correlated and thus somewhat superficial. For these tests, only the uncorrelated uncertainties (cross section, statistical, and MC statistical) are used for the model validation, the cross section extraction, and the subsequent  $\chi^2$  calculations between the fake data results and generator predictions. The removal of these fully correlated uncertainties provides a more direct test of the cross section model and its relation to the model validation procedure and cross section extraction. Since the conditional constraint tests used for validation are agnostic to the source of uncertainty, it is perhaps more useful to probe the ability of the validation to detect relevant mismodeling with a treatment of the uncertainty more akin to that of real data. Such studies, which are designed to more directly probe the ability of the model validation to detect relevant mismodeling, are presented in the Supplemental Material of [1].

The same model validation used for real data was applied to the fake data in this study. These tests expose significant disagreement between the NuWro fake data and MC prediction in the hadronic final states. This can be seen in Fig. 2(a) which shows that, analogously to real data, the  $\mu$ BooNE tune MC is unable to describe the NuWro fake data within its uncertainties. Thus, the model should be expanded before it is used to extract the desired cross sections. Using the procedure describe in Sec. VII of [1], an additional reweighting uncertainty is obtained from a reweighting function derived by unfolding the fake data with a constrained background and signal prediction and only the statistical uncertainties. This reweighting function can be seen in Fig. 2(b) alongside the one obtained from real data. The additional covariance matrix is then constructed in the same way as  $V_{\text{xs}}$  by treating the reweighted prediction as a  $1\sigma$  deviation from the original MC prediction. With this additional uncertainty applied to the MC prediction, the model shows an improved ability to describe the fake data. This is can be seen in Fig. 2(c).

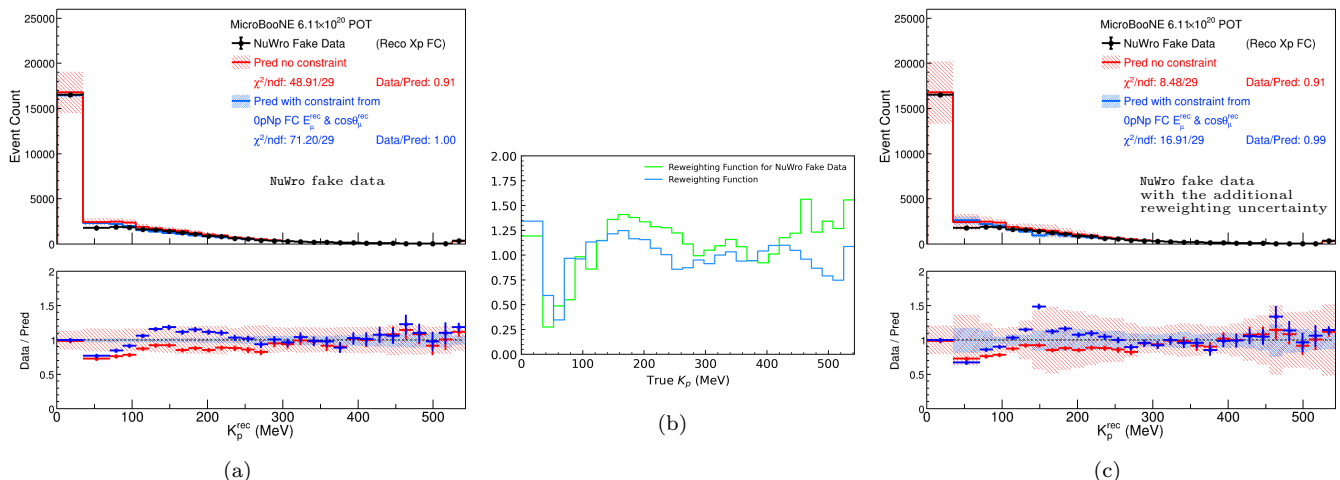


FIG. 2: (a) Fake data model validation for  $K_p^{\text{rec}}$ . Only the cross section and statistical uncertainties are included in the constraint from the muon kinematics and the calculation of the  $\chi^2$  values. This distribution does not pass model validation and motivates deriving a reweighting function to apply additional uncertainty to the fake data. This reweighting function can be seen in (b) next to the one for real data. (c) shows the same  $K_p^{\text{rec}}$  distribution and constraint as (a), but with the addition reweighting systematic applied. The improved  $\chi^2$  shows that the reweighting is sufficient for  $K_p^{\text{rec}}$ .

The results of the  $K_p$  and  $0pNp$   $E_\mu$  and  $\cos\theta_\mu$  double-differential fake data cross section extractions are presented in Figs. 3 and 4. These plots contain the extracted fake data differential cross section as well as NuWro 19.02.2 (NuWro),  $\mu$ BooNE tune, GiBUU 2023 (GiBUU), GENIE v3.0.6 G18\_10a\_02.11a (GENIE), and NEUT 5.4.0.1 (NEUT) predictions. Each generator prediction has been smeared with the  $A_C$  matrix obtained from unfolding the fake data. The NuWro prediction corresponds to the same generator configuration as used to produce the fake data but was generated independently and at higher stats than the fake data, which, at  $6.11 \times 10^{20}$  POT, is comparable in size to the real data set. Thus closure of these fake data studies is achieved when the extracted result shows good agreement with this prediction. This is indeed the case in Figs. 3 and 4, with the extracted fake data cross section agreeing better with the NuWro prediction (red dotted line) than with any other generator. The  $0p$ ,  $Np$  and  $0pNp$   $\chi^2/ndf$  values are also around or below unity and the NuWro prediction falls within  $1\sigma$  of the extracted results on almost all bins. The success of these fake data studies serve as an example of how the model validation and subsequent model expansion can be used to mitigate the potential for biased cross section results. Together, these fake data studies and the ones presented in the Supplemental Material of [1] serve as a thorough test of the model validation, model expansion, and unfolding, giving us confidence that our overall methodology is robust.

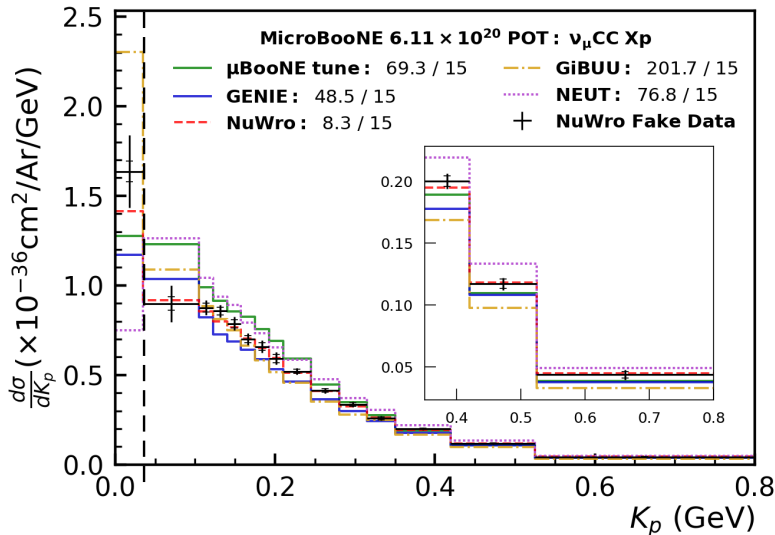


FIG. 3: Unfolded NuWro fake data  $K_p$  differential cross section result. The dashed line indicates the 35 MeV proton tracking threshold, below which is a single bin that includes events with no protons and events where the leading proton is below the threshold. The inner error bars on the data points represent the data statistical uncertainty and the outer error bars represent the uncertainty given by the square root of the diagonal elements of the extracted covariance matrix that includes only the statistical, cross section and reweighting systematics. Different generator predictions are indicated by the colored lines with corresponding  $\chi^2$  values displayed in the legend. These predictions are smeared with  $A_C$  obtained in unfolding the fake data. The inset show a magnified view of the last three bins.

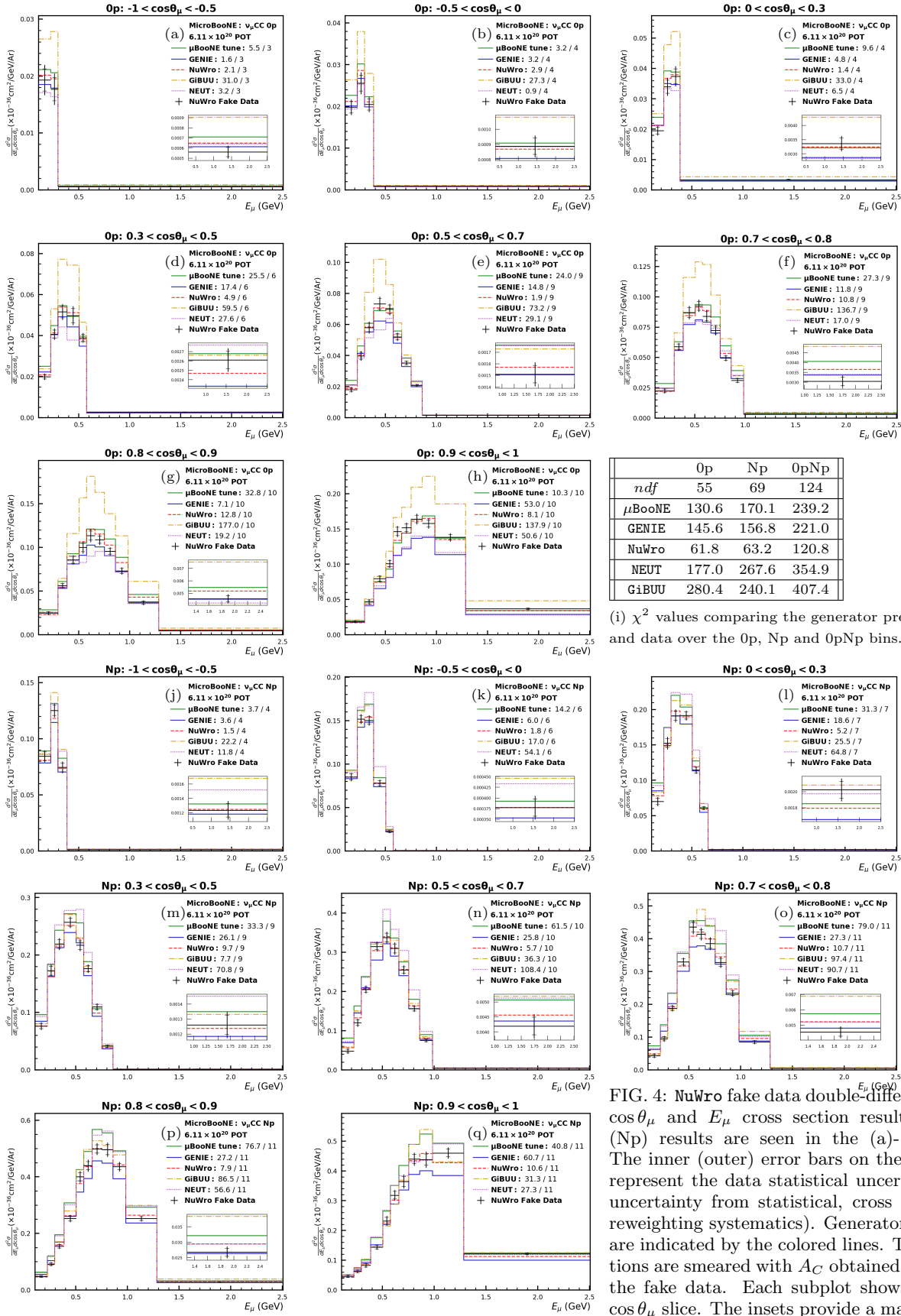


FIG. 4: NuWro fake data double-differential OpNp  $\cos\theta_\mu$  and  $E_\mu$  cross section results. The Op (Np) results are seen in the (a)-(h) [(j)-(q)]. The inner (outer) error bars on the data points represent the data statistical uncertainty (total uncertainty from statistical, cross section, and reweighting systematics). Generator predictions are indicated by the colored lines. These predictions are smeared with  $A_C$  obtained in unfolding the fake data. Each subplot shows a different  $\cos\theta_\mu$  slice. The insets provide a magnified view of the highest energy bin in a given slice.

### III. SINGLE-DIFFERENTIAL MEASUREMENTS

Analogous to the Xp double-differential measurement seen in Fig. 1(a) of the main text, the single-differential  $\cos\theta_\mu$  and  $E_\mu$  cross section measurements are presented in this section. The  $E_\mu$  result can be seen in Fig. 5 and the  $\cos\theta_\mu$  result can be seen in Fig. 6. The single-differential 0pNp measurements analogous to the double-differential ones seen in Figs. 1(b) and 1(c) of the main text can be found in [1].

Similar to the double-differential case, the single-differential Xp cross section results look fairly similar to the Np ones due to the larger Np cross section. Nevertheless, the single-differential Xp results display some differences compared to the 0pNp results in term of agreement with generators. These differences are consistent with what is observed for the double-differential measurements. In particular, as seen in Fig. 6, NEUT describes the data best for Xp  $\cos\theta_\mu$ , but the worst for 0pNp  $\cos\theta_\mu$ . Conversely, GiBUU describes Xp  $\cos\theta_\mu$  noticeably worse than 0pNp. NEUT also does significantly better for Xp  $E_\mu$  than for 0pNp  $E_\mu$ , though GiBUU and the  $\mu$ BooNE tune offer similar levels of agreement, which can be seen in Fig. 5. The underprediction of all generators at the peak of the  $E_\mu$  distribution appears more prominent for the Xp measurement than the Np one, which is not surprising due to the consistent observation of the feature in the Np channel and consistent observation of a data excess for all but GiBUU in the 0p channel.

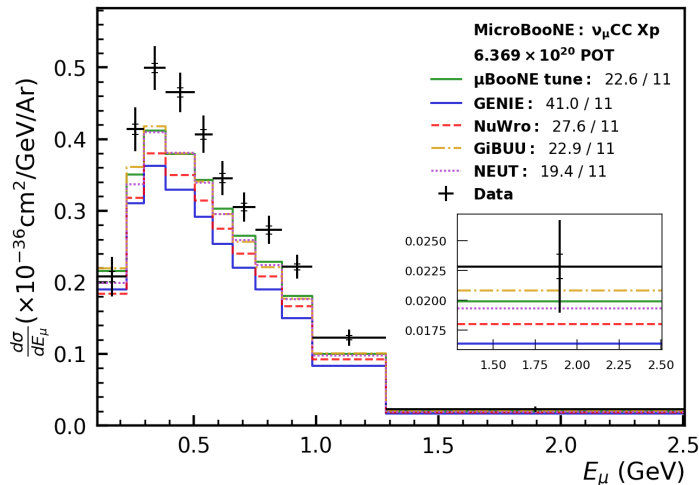


FIG. 5: Unfolded Xp  $E_\mu$  differential cross section result. The inner error bars on the data points represent the data statistical uncertainty and the outer error bars represent the uncertainty given by the square root of the diagonal elements of the extracted covariance matrix. Different generator predictions are indicated by the colored lines with corresponding  $\chi^2$  values displayed in the legend. These predictions are smeared with  $A_C$  obtained in the unfolding. The inset provides a magnified view of the most energetic bin.

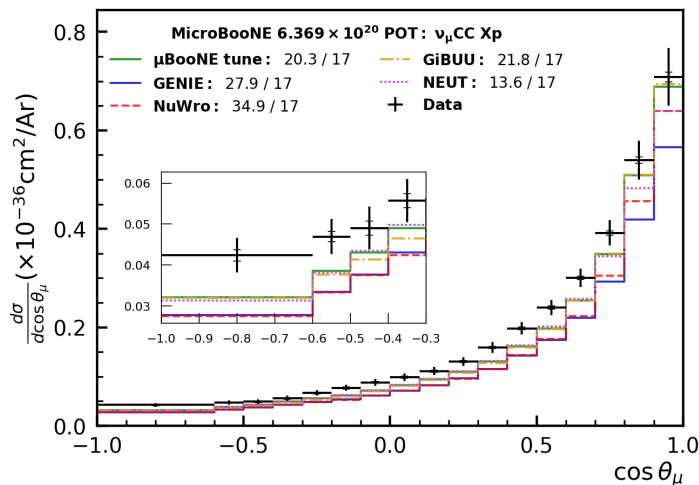


FIG. 6: Unfolded Xp  $\cos\theta_\mu$  differential cross section result. The inner error bars on the data points represent the data statistical uncertainty and the outer error bars represent the uncertainty given by the square root of the diagonal elements of the extracted covariance matrix. Different generator predictions are indicated by the colored lines with corresponding  $\chi^2$  values displayed in the legend. These predictions are smeared with  $A_C$  obtained in the unfolding. The inset provides a magnified view of the backwards bins.

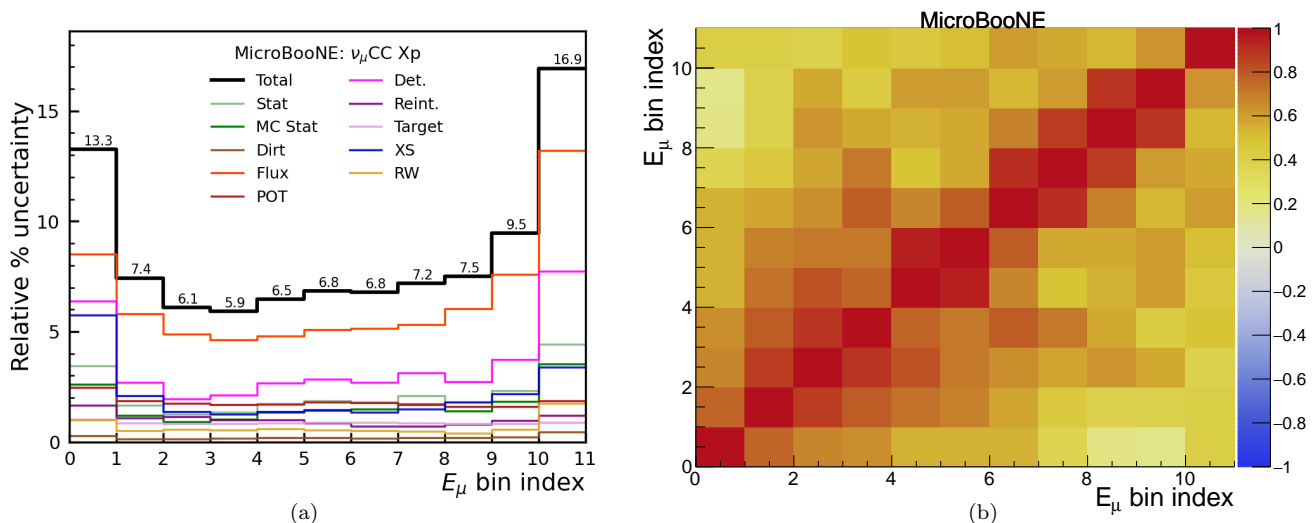


FIG. 7: (a) Contribution of uncertainties by systematic type for the extraction of the Xp differential cross section as a function of  $E_\mu$ . (b) The correlation matrix obtained from the extraction of the Xp differential cross section as a function of  $E_\mu$ . For both plots, the true bins are those found in Sec. IV and are the same as those on the extracted cross section. The entries shown in (a) correspond to the square root of the diagonal elements of the covariance matrix obtained from unfolding divided by the value of the extracted cross section for the given bin.

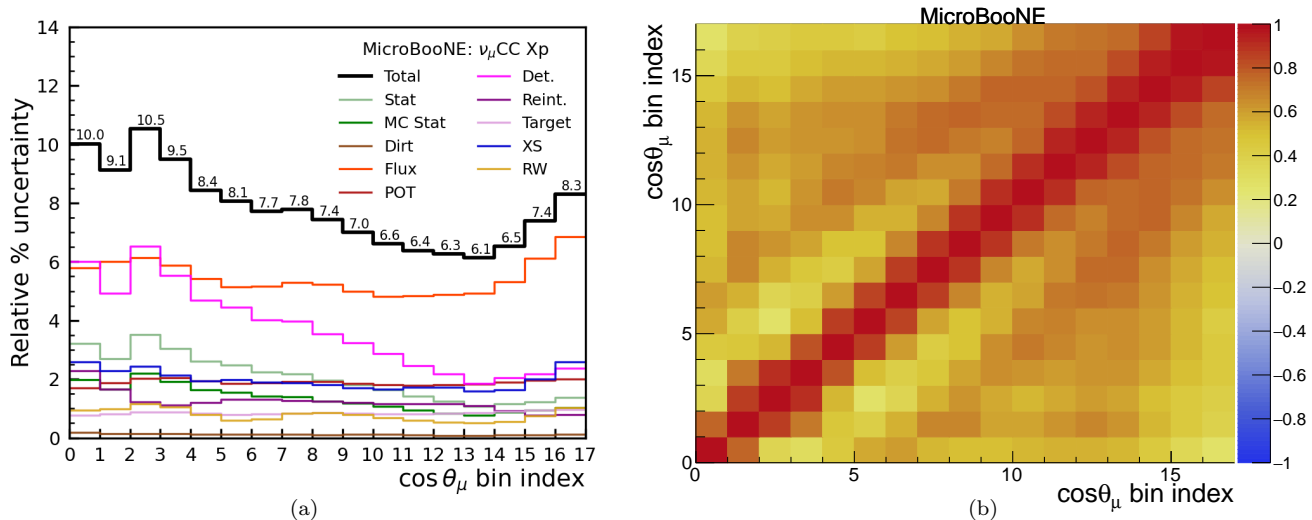


FIG. 8: (a) Contribution of uncertainties by systematic type for the extraction of the Xp differential cross section as a function of  $\cos\theta_\mu$ . (b) The correlation matrix obtained from the extraction of the Xp differential cross section as a function of  $\cos\theta_\mu$ . For both plots, the true bins are those found in Sec. IV and are the same as those on the extracted cross section. The entries shown in (a) correspond to the square root of the diagonal elements of the covariance matrix obtained from unfolding divided by the value of the extracted cross section for the given bin.

#### IV. DATA RELEASE

The unfolded cross section results shown in the main text and Sec. III can be found tabulated below. The total uncertainty, corresponding to the square root of the diagonal elements of the extracted covariance matrix, is shown for each bin. The extracted cross section results and corresponding covariance matrices can be found in a machine-readable form in `xs.txt` and `cov.txt`, respectively. The measurements from [1] are also included. The additional smearing matrix,  $A_C$ , obtained from the Wiener-SVD unfolding can be found in the same format in `Ac.txt`. Any theory or event generator prediction should be multiplied by the additional smearing matrix when comparing to this data. These files are presented in a blockwise fashion with inter-variable correlations obtained via the blockwise unfolding procedure described in [2] and in Sec. III B of [1]. The Global Bin index listed in the following tables

corresponds to the location of the bin in the blockwise covariance matrix and the Bin index corresponds to the location within the given measurement.

An example script in `gen_compare_demo.C` demonstrating how to compare the data to an external prediction is also included. This script loads the various data release files into `ROOT TMatrixD` and `TVectorD` objects. It then compares the data to an external prediction contained in `pred.txt`, which in this case is the `μBooNE` tune MC, by first smearing the prediction and then calculating  $\chi^2$  values for various measurements. More information on the files and their usage can be found in `readme.txt`.

The nominal muon neutrino flux spectrum of the Fermilab Booster Neutrino Beam at the MicroBooNE detector location can be found in `numu_flux.txt`. The results in `xs.txt` are averaged over this reference flux. External cross section predictions should likewise be averaged over this flux distribution. Note that for the total cross section reported in Fig. 25 of [1], the results are averaged over the flux from 0.2 to 4 GeV. This yields a total integrated flux of  $4.268 \times 10^{11}$  in units of number of neutrinos per  $\text{cm}^2$  for an exposure of  $6.369 \times 10^{20}$  protons on target. Similarly, for the results shown in Fig. 20 of [1], each bin is averaged over the range of the flux corresponding to the given bin. All other results have the flux integral extend over the entirety of the BNB flux. This yields a total integrated flux of  $4.586 \times 10^{11}$  in units of number of neutrinos per  $\text{cm}^2$  for an exposure of  $6.369 \times 10^{20}$  protons on target. Neutrino flux uncertainties are fully accounted for in the extracted covariance matrix and do not need to be included in theory or event generator predictions when comparing to the results. More information on `numu_flux.txt` can be found in `readme.txt`.

$K_p$ differential cross section					
Global Bin	Bin	$K_p$ Low (GeV)	$K_p$ High (GeV)	$\frac{d\sigma}{dK_p}$ ( $\times 10^{-36} \frac{\text{cm}^2}{\text{Ar GeV}}$ )	Uncertainty ( $\times 10^{-36} \frac{\text{cm}^2}{\text{Ar GeV}}$ )
99	0	0	0.035	1.9323	0.3621
100	1	0.035	0.105	1.0636	0.1443
101	2	0.105	0.1225	1.0174	0.1056
102	3	0.1225	0.14	0.9820	0.0989
103	4	0.14	0.1575	0.8981	0.1072
104	5	0.1575	0.175	0.7884	0.0912
105	6	0.175	0.1925	0.7312	0.0739
106	7	0.1925	0.21	0.6157	0.0692
107	8	0.21	0.245	0.5464	0.0508
108	9	0.245	0.28	0.4212	0.0397
109	10	0.28	0.315	0.3387	0.0322
110	11	0.315	0.35	0.2589	0.0270
111	12	0.35	0.42	0.1994	0.0198
112	13	0.42	0.525	0.1136	0.0139
113	14	0.525	0.8	0.0335	0.0117

TABLE I: Unfolded  $K_p$  differential cross section result. Bin describes the binning structure for the given measurement and Global Bin describes the binning structure used in the blockwise covariance matrix. Uncertainty corresponds to the square root of the diagonal elements of the extracted covariance matrix.

$0pNp \cos \theta_\mu$ and $E_\mu$ double-differential cross section							
Global Bin	Bin	$\cos \theta_\mu$ Low	$\cos \theta_\mu$ High	$E_\mu$ Low (GeV)	$E_\mu$ High (GeV)	$\frac{d^2\sigma}{d \cos \theta_\mu dE_\mu}$ ( $\times 10^{-36} \frac{\text{cm}^2}{\text{Ar GeV}}$ )	Uncertainty ( $\times 10^{-36} \frac{\text{cm}^2}{\text{Ar GeV}}$ )
0p							
138	0	-1	-0.5	0.106	0.226	0.00652	0.00227
139	1	-1	-0.5	0.226	0.296	0.01443	0.00341
140	2	-1	-0.5	0.296	2.506	0.00053	0.00010
141	3	-0.5	0	0.106	0.226	0.00615	0.00254
142	4	-0.5	0	0.226	0.296	0.02031	0.00415

continued on next page

continued from previous page							
Global Bin	Bin	$\cos \theta_\mu$ Low	$\cos \theta_\mu$ High	$E_\mu$ Low (GeV)	$E_\mu$ High (GeV)	$\frac{d^2\sigma}{d \cos \theta_\mu dE_\mu}$ ( $\times 10^{-36} \frac{\text{cm}^2}{\text{Ar GeV}}$ )	Uncertainty ( $\times 10^{-36} \frac{\text{cm}^2}{\text{Ar GeV}}$ )
143	5	-0.5	0	0.296	0.386	0.01580	0.00246
144	6	-0.5	0	0.386	2.506	0.00067	0.00010
145	7	0	0.3	0.106	0.226	0.00554	0.00242
146	8	0	0.3	0.226	0.296	0.02283	0.00504
147	9	0	0.3	0.296	0.386	0.02476	0.00352
148	10	0	0.3	0.386	2.506	0.00235	0.00043
149	11	0.3	0.5	0.106	0.226	0.00520	0.00213
150	12	0.3	0.5	0.226	0.296	0.02290	0.00535
151	13	0.3	0.5	0.296	0.386	0.03408	0.00511
152	14	0.3	0.5	0.386	0.505	0.03759	0.00634
153	15	0.3	0.5	0.505	0.577	0.03076	0.00356
154	16	0.3	0.5	0.577	2.506	0.00200	0.00022
155	17	0.5	0.7	0.106	0.226	0.00533	0.00228
156	18	0.5	0.7	0.226	0.296	0.02082	0.00618
157	19	0.5	0.7	0.296	0.386	0.03998	0.00754
158	20	0.5	0.7	0.386	0.505	0.06162	0.00772
159	21	0.5	0.7	0.505	0.577	0.06453	0.00732
160	22	0.5	0.7	0.577	0.659	0.04579	0.00535
161	23	0.5	0.7	0.659	0.753	0.02669	0.00314
162	24	0.5	0.7	0.753	0.861	0.01302	0.00162
163	25	0.5	0.7	0.861	2.506	0.00094	0.00016
164	26	0.7	0.8	0.106	0.296	0.00712	0.00289
165	27	0.7	0.8	0.296	0.386	0.03687	0.00581
166	28	0.7	0.8	0.386	0.505	0.07374	0.00879
167	29	0.7	0.8	0.505	0.577	0.09042	0.00922
168	30	0.7	0.8	0.577	0.659	0.08027	0.00927
169	31	0.7	0.8	0.659	0.753	0.05918	0.00694
170	32	0.7	0.8	0.753	0.861	0.03405	0.00411
171	33	0.7	0.8	0.861	0.984	0.02128	0.00329
172	34	0.7	0.8	0.984	2.506	0.00232	0.00042
173	35	0.8	0.9	0.106	0.296	0.00426	0.00289
174	36	0.8	0.9	0.296	0.386	0.02919	0.00626
175	37	0.8	0.9	0.386	0.505	0.07524	0.01074
176	38	0.8	0.9	0.505	0.577	0.10432	0.01162
177	39	0.8	0.9	0.577	0.659	0.11531	0.01198
178	40	0.8	0.9	0.659	0.753	0.10733	0.01210
179	41	0.8	0.9	0.753	0.861	0.09633	0.00947
180	42	0.8	0.9	0.861	0.984	0.07758	0.00803
181	43	0.8	0.9	0.984	1.285	0.03987	0.00471
182	44	0.8	0.9	1.285	2.506	0.00417	0.00060
183	45	0.9	1	0.106	0.296	0.00088	0.00239
184	46	0.9	1	0.296	0.386	0.02101	0.00740
185	47	0.9	1	0.386	0.505	0.06760	0.01272
186	48	0.9	1	0.505	0.577	0.09532	0.01260
187	49	0.9	1	0.577	0.659	0.12443	0.01517
188	50	0.9	1	0.659	0.753	0.16087	0.01426
189	51	0.9	1	0.753	0.861	0.21292	0.01773
190	52	0.9	1	0.861	0.984	0.22278	0.01964
191	53	0.9	1	0.984	1.285	0.18994	0.01699

continued on next page



continued from previous page							
Global Bin	Bin	$\cos \theta_\mu$ Low	$\cos \theta_\mu$ High	$E_\mu$ Low (GeV)	$E_\mu$ High (GeV)	$\frac{d^2\sigma}{d \cos \theta_\mu dE_\mu}$ ( $\times 10^{-36} \frac{\text{cm}^2}{\text{Ar GeV}}$ )	Uncertainty ( $\times 10^{-36} \frac{\text{cm}^2}{\text{Ar GeV}}$ )
192	54	0.9	1	1.285	2.506	0.03650	0.00555
Np							
193	55	-1	-0.5	0.106	0.226	0.07747	0.01481
194	56	-1	-0.5	0.226	0.296	0.19303	0.01547
195	57	-1	-0.5	0.296	0.386	0.10229	0.00950
196	58	-1	-0.5	0.386	2.506	0.00068	0.00023
197	59	-0.5	0	0.106	0.226	0.06534	0.01360
198	60	-0.5	0	0.226	0.296	0.18816	0.01535
199	61	-0.5	0	0.296	0.386	0.21169	0.01533
200	62	-0.5	0	0.386	0.505	0.09339	0.00992
201	63	-0.5	0	0.505	0.577	0.02200	0.00312
202	64	-0.5	0	0.577	2.506	0.00032	0.00006
203	65	0	0.3	0.106	0.226	0.06428	0.01432
204	66	0	0.3	0.226	0.296	0.20691	0.01967
205	67	0	0.3	0.296	0.386	0.25428	0.02058
206	68	0	0.3	0.386	0.505	0.22566	0.01984
207	69	0	0.3	0.505	0.577	0.13428	0.01354
208	70	0	0.3	0.577	0.659	0.06307	0.00851
209	71	0	0.3	0.659	2.506	0.00172	0.00029
210	72	0.3	0.5	0.106	0.226	0.05595	0.01296
211	73	0.3	0.5	0.226	0.296	0.18944	0.02119
212	74	0.3	0.5	0.296	0.386	0.22124	0.02498
213	75	0.3	0.5	0.386	0.505	0.31043	0.02557
214	76	0.3	0.5	0.505	0.577	0.31372	0.02661
215	77	0.3	0.5	0.577	0.659	0.22918	0.01882
216	78	0.3	0.5	0.659	0.753	0.11224	0.01325
217	79	0.3	0.5	0.753	0.861	0.03749	0.00511
218	80	0.3	0.5	0.861	2.506	0.00107	0.00016
219	81	0.5	0.7	0.106	0.226	0.04575	0.01328
220	82	0.5	0.7	0.226	0.296	0.18302	0.02160
221	83	0.5	0.7	0.296	0.386	0.25710	0.02510
222	84	0.5	0.7	0.386	0.505	0.38117	0.03033
223	85	0.5	0.7	0.505	0.577	0.46728	0.03311
224	86	0.5	0.7	0.577	0.659	0.42578	0.02905
225	87	0.5	0.7	0.659	0.753	0.28779	0.02646
226	88	0.5	0.7	0.753	0.861	0.15137	0.01807
227	89	0.5	0.7	0.861	0.984	0.07251	0.01042
228	90	0.5	0.7	0.984	2.506	0.00433	0.00074
229	91	0.7	0.8	0.106	0.226	0.02394	0.01070
230	92	0.7	0.8	0.226	0.296	0.11359	0.01892
231	93	0.7	0.8	0.296	0.386	0.24990	0.02425
232	94	0.7	0.8	0.386	0.505	0.36976	0.03423
233	95	0.7	0.8	0.505	0.577	0.49966	0.04173
234	96	0.7	0.8	0.577	0.659	0.54037	0.04080
235	97	0.7	0.8	0.659	0.753	0.47126	0.04263
236	98	0.7	0.8	0.753	0.861	0.38377	0.03425
237	99	0.7	0.8	0.861	0.984	0.26227	0.02778
238	100	0.7	0.8	0.984	1.285	0.10295	0.01443
239	101	0.7	0.8	1.285	2.506	0.00513	0.00087

continued on next page

continued from previous page							
Global Bin	Bin	$\cos \theta_\mu$ Low	$\cos \theta_\mu$ High	$E_\mu$ Low	$E_\mu$ High	$\frac{d^2\sigma}{d \cos \theta_\mu dE_\mu}$	Uncertainty
				(GeV)	(GeV)	$(\times 10^{-36} \frac{\text{cm}^2}{\text{Ar GeV}})$	$(\times 10^{-36} \frac{\text{cm}^2}{\text{Ar GeV}})$
240	102	0.8	0.9	0.106	0.226	0.00678	0.00879
241	103	0.8	0.9	0.226	0.296	0.06822	0.01689
242	104	0.8	0.9	0.296	0.386	0.18117	0.02210
243	105	0.8	0.9	0.386	0.505	0.29558	0.03151
244	106	0.8	0.9	0.505	0.577	0.40656	0.03920
245	107	0.8	0.9	0.577	0.659	0.45926	0.04662
246	108	0.8	0.9	0.659	0.753	0.55078	0.05271
247	109	0.8	0.9	0.753	0.861	0.61614	0.05275
248	110	0.8	0.9	0.861	0.984	0.48886	0.04749
249	111	0.8	0.9	0.984	1.285	0.29180	0.03358
250	112	0.8	0.9	1.285	2.506	0.02866	0.00499
251	113	0.9	1	0.106	0.226	0.00120	0.00901
252	114	0.9	1	0.226	0.296	0.03343	0.01405
253	115	0.9	1	0.296	0.386	0.08148	0.01665
254	116	0.9	1	0.386	0.505	0.16937	0.01846
255	117	0.9	1	0.505	0.577	0.20494	0.03159
256	118	0.9	1	0.577	0.659	0.23187	0.04205
257	119	0.9	1	0.659	0.753	0.35676	0.04281
258	120	0.9	1	0.753	0.861	0.56180	0.04363
259	121	0.9	1	0.861	0.984	0.45531	0.06002
260	122	0.9	1	0.984	1.285	0.43240	0.05498
261	123	0.9	1	1.285	2.506	0.09820	0.01936

TABLE II: Unfolded  $0pNp$   $\cos \theta_\mu$  and  $E_\mu$  double-differential cross section results. Bin describes the binning structure for the given measurement and Global Bin describes the binning structure used in the blockwise covariance matrix. Uncertainty corresponds to the square root of the diagonal elements of the extracted covariance matrix.

Xp $\cos \theta_\mu$ and $E_\mu$ double-differential cross section							
Global Bin	Bin	$\cos \theta_\mu$ Low	$\cos \theta_\mu$ High	$E_\mu$ Low (GeV)	$E_\mu$ High (GeV)	$\frac{d^2\sigma}{d \cos \theta_\mu dE_\mu}$ ( $\times 10^{-36} \frac{\text{cm}^2}{\text{Ar GeV}}$ )	Uncertainty ( $\times 10^{-36} \frac{\text{cm}^2}{\text{Ar GeV}}$ )
386	0	-1	-0.5	0.106	0.226	0.1229	0.0226
387	1	-1	-0.5	0.226	0.296	0.1938	0.0203
388	2	-1	-0.5	0.296	0.386	0.1358	0.0145
389	3	-1	-0.5	0.386	2.506	0.0012	0.0004
390	4	-0.5	0	0.106	0.226	0.1225	0.0148
391	5	-0.5	0	0.226	0.296	0.2292	0.0163
392	6	-0.5	0	0.296	0.386	0.2393	0.0180
393	7	-0.5	0	0.386	0.505	0.1074	0.0125
394	8	-0.5	0	0.505	0.577	0.0240	0.0050
395	9	-0.5	0	0.577	2.506	0.0006	0.0006
396	10	0	0.3	0.106	0.226	0.0911	0.0252
397	11	0	0.3	0.226	0.296	0.2456	0.0271
398	12	0	0.3	0.296	0.386	0.2995	0.0266
399	13	0	0.3	0.386	0.505	0.3057	0.0226
400	14	0	0.3	0.505	0.577	0.1576	0.0264
401	15	0	0.3	0.577	0.659	0.0513	0.0084
402	16	0	0.3	0.659	2.506	0.0012	0.0016
403	17	0.3	0.5	0.106	0.226	0.0758	0.0318
404	18	0.3	0.5	0.226	0.296	0.2386	0.0342
405	19	0.3	0.5	0.296	0.386	0.3242	0.0327
406	20	0.3	0.5	0.386	0.505	0.4264	0.0326
407	21	0.3	0.5	0.505	0.577	0.3572	0.0317
408	22	0.3	0.5	0.577	0.659	0.2707	0.0195
409	23	0.3	0.5	0.659	0.753	0.1428	0.0120
410	24	0.3	0.5	0.753	0.861	0.0528	0.0072
411	25	0.3	0.5	0.861	2.506	0.0026	0.0014
412	26	0.5	0.7	0.106	0.226	0.0619	0.0258
413	27	0.5	0.7	0.226	0.296	0.2152	0.0274
414	28	0.5	0.7	0.296	0.386	0.3253	0.0293
415	29	0.5	0.7	0.386	0.505	0.4917	0.0362
416	30	0.5	0.7	0.505	0.577	0.5129	0.0451
417	31	0.5	0.7	0.577	0.659	0.5024	0.0360
418	32	0.5	0.7	0.659	0.753	0.3813	0.0355
419	33	0.5	0.7	0.753	0.861	0.1954	0.0278
420	34	0.5	0.7	0.861	0.984	0.0758	0.0115
421	35	0.5	0.7	0.984	2.506	0.0088	0.0041
422	36	0.7	0.8	0.106	0.226	0.0155	0.0245
423	37	0.7	0.8	0.226	0.296	0.1562	0.0265
424	38	0.7	0.8	0.296	0.386	0.3147	0.0319
425	39	0.7	0.8	0.386	0.505	0.4913	0.0365
426	40	0.7	0.8	0.505	0.577	0.6139	0.0478
427	41	0.7	0.8	0.577	0.659	0.6881	0.0528
428	42	0.7	0.8	0.659	0.753	0.6334	0.0530
429	43	0.7	0.8	0.753	0.861	0.4702	0.0476
430	44	0.7	0.8	0.861	0.984	0.2958	0.0355
431	45	0.7	0.8	0.984	1.285	0.1321	0.0168
432	46	0.7	0.8	1.285	2.506	0.0201	0.0047
433	47	0.8	0.9	0.106	0.226	0.0172	0.0185
434	48	0.8	0.9	0.226	0.296	0.1443	0.0232

continued on next page

continued from previous page							
Global Bin	Bin	$\cos \theta_\mu$ Low	$\cos \theta_\mu$ High	$E_\mu$ Low	$E_\mu$ High	$\frac{d^2\sigma}{d \cos \theta_\mu E_\mu}$	Uncertainty
				(GeV)	(GeV)	$(\times 10^{-36} \frac{\text{cm}^2}{\text{Ar GeV}})$	$(\times 10^{-36} \frac{\text{cm}^2}{\text{Ar GeV}})$
435	49	0.8	0.9	0.296	0.386	0.2494	0.0291
436	50	0.8	0.9	0.386	0.505	0.3655	0.0400
437	51	0.8	0.9	0.505	0.577	0.5536	0.0454
438	52	0.8	0.9	0.577	0.659	0.6248	0.0572
439	53	0.8	0.9	0.659	0.753	0.7094	0.0566
440	54	0.8	0.9	0.753	0.861	0.7089	0.0577
441	55	0.8	0.9	0.861	0.984	0.5810	0.0581
442	56	0.8	0.9	0.984	1.285	0.3292	0.0288
443	57	0.8	0.9	1.285	2.506	0.0614	0.0099
444	58	0.9	1	0.106	0.226	0.0206	0.0194
445	59	0.9	1	0.226	0.296	0.0865	0.0261
446	60	0.9	1	0.296	0.386	0.1102	0.0272
447	61	0.9	1	0.386	0.505	0.2818	0.0310
448	62	0.9	1	0.505	0.577	0.4142	0.0465
449	63	0.9	1	0.577	0.659	0.4093	0.0505
450	64	0.9	1	0.659	0.753	0.6005	0.0560
451	65	0.9	1	0.753	0.861	0.8366	0.0671
452	66	0.9	1	0.861	0.984	0.8516	0.0730
453	67	0.9	1	0.984	1.285	0.6476	0.0655
454	68	0.9	1	1.285	2.506	0.1755	0.0209

TABLE III: Unfolded  $X_p \cos \theta_\mu$  and  $E_\mu$  double-differential cross section result. Bin describes the binning structure for the given measurement and Global Bin describes the binning structure used in the blockwise covariance matrix. Uncertainty corresponds to the square root of the diagonal elements of the extracted covariance matrix.

Xp $E_\mu$ differential cross section						
Global Bin	Bin	$E_\mu$ Low	$E_\mu$ High	$\frac{d\sigma}{dE_\mu}$	Uncertainty	
		(GeV)	(GeV)	$(\times 10^{-36} \frac{\text{cm}^2}{\text{Ar GeV}})$	$(\times 10^{-36} \frac{\text{cm}^2}{\text{Ar GeV}})$	
358	0	0.106	0.226	0.2080	0.0276	
359	1	0.226	0.296	0.4137	0.0307	
360	2	0.296	0.386	0.4994	0.0304	
361	3	0.386	0.505	0.4652	0.0275	
362	4	0.505	0.577	0.4068	0.0263	
363	5	0.577	0.659	0.3455	0.0236	
364	6	0.659	0.753	0.3051	0.0207	
365	7	0.753	0.861	0.2730	0.0196	
366	8	0.861	0.984	0.2215	0.0166	
367	9	0.984	1.285	0.1226	0.0116	
368	10	1.285	2.506	0.0228	0.0039	

TABLE IV: Unfolded  $E_\mu$  differential cross section result. Bin describes the binning structure for the given measurement and Global Bin describes the binning structure used in the blockwise covariance matrix. Uncertainty corresponds to the square root of the diagonal elements of the extracted covariance matrix.

Xp $\cos \theta_\mu$ differential cross section					
Global Bin	Bin	$\cos \theta_\mu$ Low	$\cos \theta_\mu$ High	$\frac{d\sigma}{d \cos \theta_\mu}$ ( $\times 10^{-36} \frac{\text{cm}^2}{\text{Ar}}$ )	Uncertainty ( $\times 10^{-36} \frac{\text{cm}^2}{\text{Ar}}$ )
369	0	-1	-0.6	0.0423	0.0042
370	1	-0.6	-0.5	0.0469	0.0043
371	2	-0.5	-0.4	0.0490	0.0052
372	3	-0.4	-0.3	0.0557	0.0053
373	4	-0.3	-0.2	0.0667	0.0056
374	5	-0.2	-0.1	0.0771	0.0062
375	6	-0.1	0	0.0883	0.0068
376	7	0	0.1	0.0984	0.0077
377	8	0.1	0.2	0.1109	0.0082
378	9	0.2	0.3	0.1306	0.0091
379	10	0.3	0.4	0.1591	0.0105
380	11	0.4	0.5	0.1975	0.0126
381	12	0.5	0.6	0.2402	0.0151
382	13	0.6	0.7	0.3005	0.0184
383	14	0.7	0.8	0.3918	0.0256
384	15	0.8	0.9	0.5392	0.0398
385	16	0.9	1	0.7085	0.0588

TABLE V: Unfolded  $\cos \theta_\mu$  differential cross section result. Bin describes the binning structure for the given measurement and Global Bin describes the binning structure used in the blockwise covariance matrix. Uncertainty corresponds to the square root of the diagonal elements of the extracted covariance matrix.

- 
- [1] P. Abratenko *et al.* (MicroBooNE Collaboration), Inclusive cross section measurements in final states with and without protons for charged-current  $\nu_\mu$ -Ar scattering in MicroBooNE, [Phys. Rev. D \*\*110\*\*, 013006 \(2024\)](#).  
[2] S. Gardiner, Mathematical methods for neutrino cross-section extraction, arXiv preprint (2024), [arXiv:2401.04065 \[hep-ex\]](#).